Supplementary material

Cherry-picking resolvents: A general strategy for convergent coupled-cluster damped response calculations of core-level spectra

Kaushik D. Nanda[a,*] and Anna I. Krylov[a,†]

[a] Department of Chemistry, University of Southern California, Los Angeles, California 90089-0482

* kaushikdnanda@gmail.com (K.D.N.), † krylov@usc.edu (A.I.K.)

Contents

1. FC-CVS-EOM-CCSD METHOD FOR RIXS CROSS SECTIONS

We used the "frozen core" or "fc" variant of CVS-EOM-EE-CCSD[1–4]. In the fc-CVS-EOM-EE-CCSD method, the core electrons are frozen in the calculations of the CCSD amplitudes ($\mathcal{T}$) for the reference state. In the calculations of valence states, core electrons were frozen in the CCSD and in the EOM amplitudes ($\mathcal{R}$ and $\mathcal{L}$).

2. CONFIGURATIONAL ANALYSIS OF THE RESPONSE STATES AND THEIR CONTRIBUTIONS TO THE RIXS MOMENTS

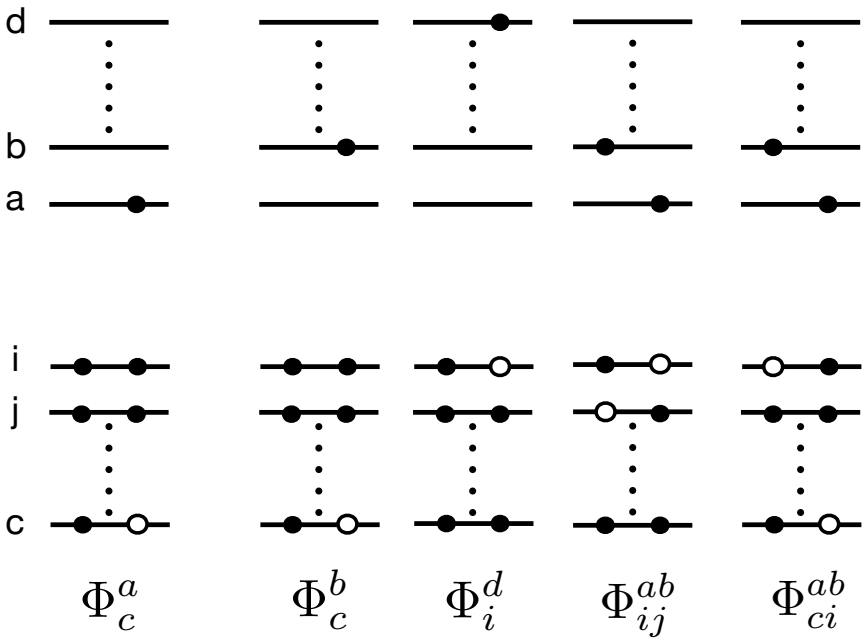

FIG. S1: Relevant electronic configurations. Index c denotes core orbital, i and j denote valence occupied orbitals, a denotes low-lying valence orbital (e.g., LUMO), b denotes a low-lying virtual orbital in the continuum, and d denotes a higher-lying virtual orbital. Configuration Φ_c^a represents core-excited state and other configurations represent configurations that can mix with it: Φ_c^b (core-excited state with one electron in a continuum orbital), Φ_i^d (high-lying valence-excited continuum state), Φ_{ij}^{ab} and Φ_{cj}^{ab} (doubly excited configurations with one electron in a continuum orbital).

What are the dominant decay channels for core-excited states? We begin with a brief configurational analysis of core-excited states. Figure S1 shows electronic configurations appearing in the full Fock space of EOM-CCSD. Configurations in which orbitals b or d are occupied represent continuum states. Φ_c^a represents core-excited state, which lies below the

core-ionization continuum, i.e., below Φ_c^b and Φ_{ci}^{ab}. Φ_c^a can decay by a two-electron process in which one valence electron fills the core hole and another valence electron is ejected (i.e., excited into a diffuse orbital d corresponding to a discretized continuum state). This decay channel is represented by the valence doubly excited configuration Φ_{ij}^{ab}. Formally, by two-electron transition, Φ_c^a can also decay into Φ_i^d (singly excited configuration in which a valence electron is excited into a very high-lying orbital d). CVS uncouples the EOM-CC Fock spaces of valence and core-excited configurations, which blocks the decay channels for Φ_c^a, making it electronically bound. However, by analyzing coupling elements between Φ_c^a and Φ_{ij}^{ab}/Φ_i^d, one can show that the decay is dominated by Φ_{ij}^{ab} whereas Φ_i^d is not relevant:

$$\langle \Phi_c^a | H | \Phi_{ij}^{ab} \rangle = \langle ij || bc \rangle \tag{1}$$

$$\langle \Phi_c^a | H | \Phi_i^d \rangle = \langle ia || dc \rangle. \tag{2}$$

Energy matching requirement means that orbital d should be very high in energy:

$$\epsilon_a - \epsilon_c \approx \epsilon_d - \epsilon_i \tag{3}$$

$$\epsilon_d = \epsilon_a + \epsilon_i - \epsilon_c, \tag{4}$$

i.e., several hundreds of electron-volts. This means that d is highly oscillatory, whether it represents a diffuse pseudo-continuum state or a localized high-lying valence-like orbital. The oscillatory character of d kills the integral in Eq. (2). Numeric experimentation[5] confirms that keeping all single excitations in the EOM-CC Fock space does not cause any numeric problems and that only valence double excitations strongly mix with core-excited states. In addition, the density of these singly excited configurations is smaller than the density of doubly excited configurations. Hence, the core CVS-EOM-CCSD Fock space can be augmented by including valence single excitations without having a significant effect on the core-excited states—neither in terms of changing their energy nor in terms of causing convergence problems.

What are the dominant excited configurations in RIXS response and the dominant orbital channels contributing to the RIXS moments? Let us now analyze Eqs. (5)–(8) from the main text in terms of anticipated leading configurations in the response states $\mathcal{X}^k$ and the magnitude of the respective contributions into the total RIXS moments. Neglecting correlation effects, we consider only dominant electronic configurations in the initial and target states, such that $\Psi^g \sim \Phi_0$ (reference determinant) and $\Psi^f \sim \Phi_i^a$ (valence excited state). Note that indices b and d now refer to virtual orbitals of any type (valence, diffuse, high-energy oscillatory). We also neglect the correlation effects entering through the similarity transformation

of μ (these effects are absent in the CISD ansatz and only appear in EOM-CC). We also assume that all dipole transitions are symmetry allowed. Note that Ψ^f is expressed only in terms of pure valence excitations, because valence excited states are described within the frozen-core (FC) approximation in the fc-CVS-EOM-CC ansatz. Table S1 and S2 summarizes the analysis.

For $M^{f\leftarrow g}$, we consider response state $\mathcal{X}^g$. Table S1 shows that the response state is dominated by single excitations because only singles directly couple to Φ_0 by the dipole moment operator. These single excitations are of two types: core-excited (Φ_c^b) and valence-excited (Φ_j^b). The corresponding coupling elements (weights of these configurations) are $\langle b|\mu|c\rangle$ and $\langle b|\mu|j\rangle$. CVS-0 includes the contributions due to Φ_c^b, but not Φ_j^b; these contributions are included in both CVS-uS and CVS-CCS (and of course in CVS-CC2).

The photon energies in RIXS typically lie below the core-ionization energy. By applying the near-resonance-enhancement argument, only the target orbitals b in Φ_c^b for which $\epsilon_b - \epsilon_c$ is nearly resonant with ω are important. Note that the RIXS response calculation also includes contributions from higher valence orbitals, their contribution to the response state is smaller due to their off-resonance and oscillatory (for high-lying continuum orbitals) character. These off-resonance contributions do not cause problems with convergence of response wave functions—in analogy to smoothly convergent response calculations in multi-photon valence processes. From the configurations in Ψ^f valence state that can contribute to via $\langle\Psi^f|\mu|\Phi_c^b\rangle$, there is only one type, i.e., Φ_j^b, that can contribute to $M^{f\leftarrow g}$. The contribution from Φ_i^a ($\in\{\Phi_j^b\}$) is expected to be large based on resonance-enhancement argument as Φ_i^a is the leading configuration in Ψ^f. The matrix elements in the numerators of sum-over-states terms of $M^{f\leftarrow g}$ for this Φ_c^b channel are then given by $\langle b|\mu|c\rangle\langle c|\mu|j\rangle$.

The second type of configurations, i.e., Φ_j^b, contributing to $\mathcal{X}^g$, corresponds to an excitation from a valence orbital j into a high-lying orbital b. These configurations can, in principle, cause problems in response equations, but we expect their density to be small in the X-ray energy range when using realistic basis sets. Their contribution to $M^{f\leftarrow g}$ is expected to be small because b is highly oscillatory (and/or off resonance), for the same reasons as explained above. The leading contribution to $M^{f\leftarrow g}$ for final state Φ_i^a can come from several configurations, but only three types survive due to FC. Note that the effect of Φ_{jk}^{bd} are typically small when d is highly oscillatory and Φ_{jk}^{bd} is not a leading configuration in Ψ^f, but in charge-transfer $k\rightarrow d$ ($k=i, d=a$) transitions with large $\langle a|\mu|i\rangle$ transition moments, these contributions can become important.

TABLE S1: Configurational analysis of the leading contributions to the RIXS moments, $M^{f\leftarrow g}$, where $\Psi^g \approx \Phi_0$ and $\Psi^f \approx \Phi_i^a$. Φ_ρ is defined as a configuration in $\langle\Phi_\rho|X^g\rangle$ and Φ_ν is the leading configuration in $\langle\Psi^f|\Phi_\nu\rangle$ that couples with Φ_ρ.

.

Φ_ρ	Φ_ν	$\frac{\langle\Psi^f\|\mu\|\Phi^\rho\rangle\langle\Phi_\rho\|\mu\|\Psi^g\rangle}{\epsilon_\rho-\epsilon_g-\omega}$	Comment
Φ_c^b	Φ_c^d	$\frac{\langle d\|\mu\|c\rangle\langle c\|\mu\|b\rangle}{\epsilon_b-\epsilon_c-\omega}$	Not present due to FC
	Φ_j^b	$\frac{\langle b\|\mu\|j\rangle\langle c\|\mu\|b\rangle}{\epsilon_b-\epsilon_c-\omega}$	Large when $b=a$, $j=i$, $\epsilon_b-\epsilon_c\approx\omega$
	Φ_{cj}^{bd}	$\frac{\langle d\|\mu\|j\rangle\langle c\|\mu\|b\rangle}{\epsilon_b-\epsilon_c-\omega}$	Not present due to FC
	$\Phi_{cc'}^{bd}$	$\frac{\langle d\|\mu\|c'\rangle\langle c\|\mu\|b\rangle}{\epsilon_b-\epsilon_c-\omega}$	Not present due to FC
Φ_j^b	Φ_c^b	$\frac{\langle b\|\mu\|c\rangle\langle j\|\mu\|b\rangle}{\epsilon_b-\epsilon_j-\omega}$	Not present due to FC
	Φ_j^d	$\frac{\langle d\|\mu\|b\rangle\langle j\|\mu\|b\rangle}{\epsilon_b-\epsilon_j-\omega}$	Large if $b=d=a$ and CT
	Φ_k^b	$\frac{\langle k\|\mu\|j\rangle\langle j\|\mu\|b\rangle}{\epsilon_b-\epsilon_j-\omega}$	Large if $j=k=i$ and CT
	Φ_{jk}^{bd}	$\frac{\langle d\|\mu\|k\rangle\langle j\|\mu\|b\rangle}{\epsilon_b-\epsilon_j-\omega}$	Small; $\epsilon_b-\epsilon_j << \omega$ or b/d are highly oscillatory
	Φ_{jc}^{bd}	$\frac{\langle d\|\mu\|c\rangle\langle j\|\mu\|b\rangle}{\epsilon_b-\epsilon_j-\omega}$	Not present due to FC

CT $\rightarrow \Psi^f=\Phi_i^a$ is a charge-transfer transition with large $\langle\Psi^f|\mu|\Psi^f\rangle$, $\langle\Psi^g|\mu|\Psi^g\rangle$, and $\langle\Psi^f|\mu|\Psi^g\rangle$

Following the same steps, the configurational analysis of $M^{g\leftarrow f}$ in Table S2 provides similar information about different channels. In this case, both singly and doubly excited configurations can contribute to the response states $\mathcal{X}^f$. The largest contributions are expected from Φ_i^b, Φ_j^a, and Φ_c^a configurations. Φ_i^b and Φ_j^a have large contributions when $b=a$ and $j=i$ for strong charge-transfer $\Psi^g\rightarrow\Psi^f$ transitions (large $\langle i|\mu|a\rangle$) with large (difference in the) permanent dipole moments of the initial and final states[6]. CVS-0 does not capture these contributions.

TABLE S2: Configurational analysis of the leading contributions to the RIXS moments, $M^{g\leftarrow f}$, where $\Psi^g \approx \Phi_0$ and $\Psi^f \approx \Phi_i^a$. Φ_ρ is defined as a configuration in $\langle\Phi_\rho|X^f\rangle$ and Φ_ν is the leading configuration in $\langle\Psi^g|\Phi_\nu\rangle$ that couples with Φ_ρ.

Φ_ρ	Φ_ν	$\frac{\langle\Psi^g\|\mu\|\Phi^\rho\rangle\langle\Phi_\rho\|\mu\|\Psi^f\rangle}{\epsilon_\rho-\epsilon_g-\omega}$	Comment
Φ_i^b	Φ_0	$\frac{\langle i\|\mu\|b\rangle\langle b\|\mu\|a\rangle}{\epsilon_b-\epsilon_i-\omega}$	Large if $b=a$ and CT
Φ_j^a	Φ_0	$\frac{\langle a\|\mu\|j\rangle\langle j\|\mu\|i\rangle}{\epsilon_a-\epsilon_j-\omega}$	Large if $j=i$ and CT
Φ_c^a	Φ_0	$\frac{\langle a\|\mu\|c\rangle\langle c\|\mu\|i\rangle}{\epsilon_a-\epsilon_c-\omega}$	Large when $\epsilon_a-\epsilon_c\approx\omega$
Φ_{ij}^{ab}	Φ_0	$\frac{0\times\langle b\|\mu\|j\rangle}{\epsilon_b-\epsilon_j+\epsilon_a-\epsilon_i-\omega}$	$\langle\Psi^g\|\mu\|\Phi_{ij}^{ab}\rangle\approx 0$ by Slater rules
Φ_{ic}^{ab}	Φ_0	$\frac{0\times\langle b\|\mu\|c\rangle}{\epsilon_b-\epsilon_i-\omega}$	$\langle\Psi^g\|\mu\|\Phi_{ic}^{ab}\rangle=0$ by Slater rules and FC

CT $\rightarrow \Psi^f=\Phi_i^a$ is a charge-transfer transition with large $\langle\Psi^f|\mu|\Psi^f\rangle$, $\langle\Psi^g|\mu|\Psi^g\rangle$, and $\langle\Psi^g|\mu|\Psi^f\rangle$

The contribution from Φ_c^b configurations is driven by the near-resonance enhancement and is captured by CVS-0. Importantly, Table S2 illustrates that the contribution of doubles into the RIXS moment is expected to be small because of the Slater rules and FC approximation applied to Ψ^f. The contribution of doubles is indirect and enters through their effect on the single amplitudes of the response equations and through the correlation part of Ψ^g. This explains generally good performance of CVS-0 and suggests that CVS-uS and CVS-CCS capture the dominant effects, providing additional justification to these approximations.

The valence double configurations, Φ_{ij}^{ab}, which can significantly contribute to $\mathcal{X}^f$ (and also $\mathcal{X}^g$ in correlated methods), are the main reason of poor convergence. The density of double excitations Φ_{ij}^{ab} is higher than the density of Φ_i^b because the energy of the former can be tuned by varying j, whereas for the latter, i is fixed and the density of states is determined by the number of available diffuse orbitals at this energy range. The quality of preconditioner for the doubles–doubles block at the photon energies used in RIXS also contributes to the convergence problems.

3. RIXS CROSS SECTIONS

3.1. Water

TABLE S3: fc-CVS-EOM-EE-CCSD valence excitation energies $\mathcal{E}_f - \mathcal{E}_0$ (eV) and RIXS cross sections σ (a.u.) for the incident photon resonant with the lowest $XA_1 \rightarrow B_2$ core excitation at 535.23 eV and scattering angle $\theta = 0°$ with the CVS-0, CVS-CCS, CVS-uS, and CVS-CC2 approaches. For the standard EOM-EE-CCSD method, excitation energies and RIXS cross sections with the incident photon energy of 535.74 eV are reported for comparison.

	EOM-EE-CCSD		fc-CVS-EOM-EE-CCSD				
Final				CVS-0	CVS-CCS	CVS-uS	CVS-CC2
State	$\mathcal{E}_f - \mathcal{E}_0$	σ	$\mathcal{E}_f - \mathcal{E}_0$	σ	σ	σ	σ
$1B_2$	7.4100	0.023556	7.4013	0.023643	0.023751	0.023754	0.023737
$1A_2$	9.1600	0.000491	9.1500	0.000180	0.000492	0.000492	0.000488
$2A_1$	9.7400	0.007563	9.7397	0.007644	0.007644	0.007645	0.007645
$2B_2$	10.0100	0.000759	10.0142	0.000053	0.000668	0.000668	0.000755
$3A_1$	10.1000	0.001288	10.0991	0.001314	0.001314	0.001314	0.001315
$3B_2$	10.3900	0.000253	10.3799	0.000257	0.000255	0.000255	0.000255
$2A_2$	10.8000	0.000015	10.7910	0.000029	0.000012	0.000012	0.000015
$4B_2$	11.2100	0.000159	11.2072	0.000009	0.000140	0.000140	0.000157
$4A_1$	11.2200	0.000011	11.2119	0.000011	0.000011	0.000011	0.000011
$5B_2$	11.3000	0.000062	11.2963	0.000060	0.000062	0.000062	0.000062
$3A_2$	11.4300	0.000038	11.4162	0.000010	0.000031	0.000031	0.000041
$1B_1$	11.5000	0.000430	11.4997	0.000130	0.000393	0.000391	0.000427
$6B_2$	11.6800	0.000092	11.6708	0.000016	0.000074	0.000074	0.000077
$5A_1$	11.6900	0.000002	11.6857	0.000002	0.000002	0.000002	0.000002
$7B_2$	11.7200	0.000076	11.7124	0.000016	0.000077	0.000077	0.000083
$4A_2$	11.8300	0.000155	11.8118	0.000005	0.000131	0.000131	0.000149
$8B_2$	12.2000	0.000641	12.2022	0.000013	0.000574	0.000574	0.000635
$6A_1$	12.2600	0.000046	12.2616	0.000045	0.000045	0.000045	0.000045

$7A_1$	12.6600	0.000113	12.6587	0.000117	0.000118	0.000118	0.000118
$9B_2$	13.0700	0.000298	13.0617	0.000191	0.000297	0.000297	0.000290

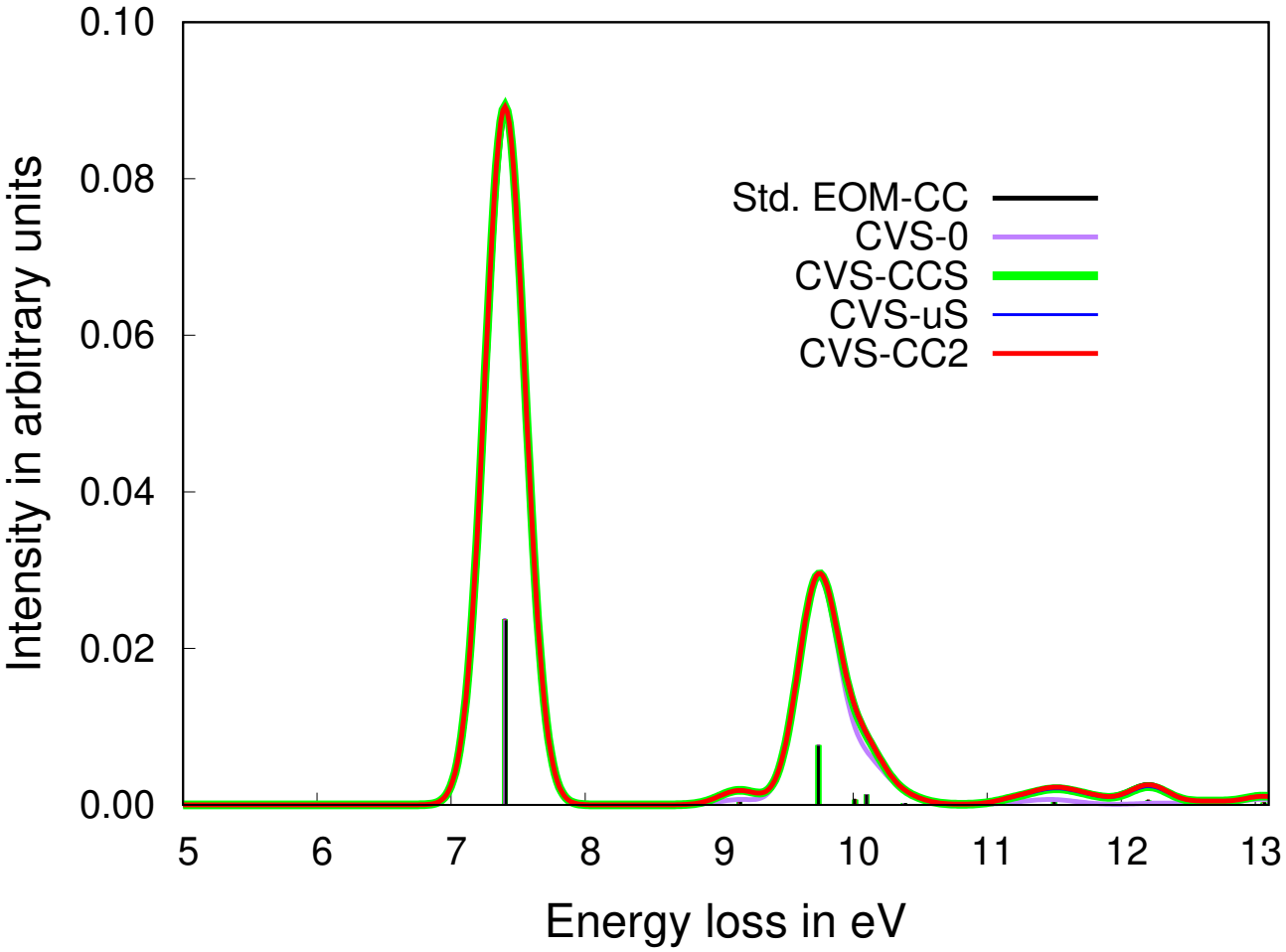

FIG. S2: RIXS emission spectra for water computed using different resolvents within the CVS-EOM-EE-CCSD framework with incident photon energy of 535.23 eV and using the standard EOM-EE-CCSD framework with incident photon energy of 535.74 eV. Scattering angle $\theta = 0°$. The spectra are convoluted using normalized Gaussians (FWHM = 0.25 eV).

3.2. Benzene

TABLE S4: fc-CVS-EOM-EE-CCSD/6-311(2+,+)G**(uC) valence excitation energies $\mathcal{E}_f - \mathcal{E}_0$ (eV) of gerade states and their RIXS cross sections σ (a.u.) for scattering angle $\theta = 0°$ with the CVS-0, CVS-CCS, CVS-uS, and CVS-CC2 approaches.

		Peak A (ω_i = 285.97 eV)				Peak B (ω_i = 287.80 eV)			
Final		CVS-0	CVS-CCS	CVS-uS	CVS-CC2	CVS-0	CVS-CCS	CVS-uS	CVS-CC2
state	$\mathcal{E}_f - \mathcal{E}_0$	σ	σ	σ	σ	σ	σ	σ	σ
XA_g	0.0000	1.271069	1.271467	1.271141	1.271380	0.038015	0.040213	0.038436	0.039810
$1B_{2g}$	6.4522	0.000203	0.000125	0.000114	0.000176	0.020322	0.020471	0.020474	0.020364
$1B_{3g}$	6.4522	0.000203	0.000360	0.000363	0.000405	0.020325	0.022597	0.022598	0.022724
$2B_{2g}$	7.5690	0.000179	0.002440	0.002443	0.002201	0.001242	0.003591	0.003595	0.003349
$2B3_g$	7.5690	0.000179	0.001848	0.001850	0.001800	0.001242	0.002960	0.002964	0.002920
$3B_{3g}$	7.6305	0.000000	0.000000	0.000000	0.000000	0.000000	0.000000	0.000000	0.000000
$3B_{2g}$	7.6380	0.000000	0.000000	0.000000	0.000000	0.000000	0.000000	0.000000	0.000000
$4B_{2g}$	7.6549	0.000005	0.000294	0.000295	0.000349	0.000097	0.000435	0.000438	0.000494
$4B_{3g}$	7.6549	0.000005	0.001768	0.001772	0.001974	0.000097	0.002011	0.002016	0.002224
$2A_g$	7.8649	0.000000	0.000000	0.000000	0.000000	0.000000	0.000000	0.000000	0.000000
$1B_{1g}$	7.8649	0.000000	0.000182	0.000185	0.000211	0.000000	0.000182	0.000185	0.000211
$3A_g$	7.8758	0.000419	0.000417	0.000415	0.000416	0.000065	0.000062	0.000058	0.000060
$2B_{1g}$	7.9077	0.000000	0.000584	0.000583	0.001081	0.000000	0.000578	0.000577	0.001070
$5B_{2g}$	8.2864	0.000092	0.000173	0.000174	0.000183	0.000538	0.000643	0.000644	0.000654
$5B_{3g}$	8.2864	0.000093	0.000205	0.000205	0.000194	0.000538	0.000684	0.000685	0.000669
$6B_{3g}$	8.8542	0.000000	0.000000	0.000000	0.000000	0.000000	0.000000	0.000000	0.000000
$6B_{2g}$	8.8694	0.000016	0.000021	0.000021	0.000041	0.000096	0.000107	0.000106	0.000130
$7B_{3g}$	8.8694	0.000016	0.000291	0.000292	0.000372	0.000096	0.000387	0.000388	0.000470
$7B_{2g}$	8.8803	0.000000	0.000000	0.000000	0.000000	0.000000	0.000000	0.000000	0.000000
$4A_g$	9.1039	0.000000	0.000001	0.000002	0.000000	0.000001	0.000001	0.000003	0.000001
$3B_{1g}$	9.1039	0.000000	0.001877	0.001902	0.001350	0.000001	0.001842	0.001867	0.001324
$8B_{2g}$	9.1832	0.000000	0.000000	0.000000	0.000000	0.000000	0.000000	0.000000	0.000000

$9B_{2g}$	9.1945	0.000054	0.000052	0.000052	0.000053	0.000091	0.000091	0.000090	0.000094
$8B_{3g}$	9.1945	0.000054	0.000069	0.000069	0.000085	0.000091	0.000109	0.000109	0.000128
$9B_{3g}$	9.2040	0.000000	0.000000	0.000000	0.000000	0.000000	0.000000	0.000000	0.000000
$5A_g$	9.2312	0.000000	0.000005	0.000010	0.000001	0.000020	0.000023	0.000027	0.000020
$4B_{1g}$	9.2312	0.000000	0.004870	0.004936	0.002932	0.000020	0.004757	0.004821	0.002860
$6A_g$	9.3171	0.000000	0.000000	0.000000	0.000000	0.000036	0.000036	0.000034	0.000037
$5B_{1g}$	9.3171	0.000000	0.000419	0.000428	0.000585	0.000036	0.000351	0.000358	0.000496
$10B_{2g}$	9.6038	0.001500	0.001787	0.001788	0.001693	0.000113	0.000316	0.000318	0.000241
$10B_{3g}$	9.6038	0.001500	0.001663	0.001663	0.001630	0.000113	0.000186	0.000186	0.000174
$7A_g$	10.0565	0.000000	0.000000	0.000001	0.000000	0.000001	0.000001	0.000002	0.000001
$6B_{1g}$	10.0565	0.000000	0.000000	0.000001	0.000000	0.000001	0.000001	0.000002	0.000001
$8A_g$	10.1277	0.000985	0.000994	0.000983	0.001003	0.000344	0.000351	0.000341	0.000358
$7B_{1g}$	10.1657	0.000000	0.001714	0.001709	0.003423	0.000000	0.001695	0.001691	0.003384
$9A_g$	10.4176	0.000042	0.000038	0.000032	0.000045	0.001101	0.001098	0.001093	0.001103
$8B_{1g}$	10.4176	0.000042	0.000609	0.000622	0.000619	0.001101	0.001730	0.001741	0.001740
$11B_{2g}$	10.4322	0.000249	0.000224	0.000222	0.000254	0.002642	0.002639	0.002638	0.002643
$11B_{3g}$	10.4322	0.000249	0.000181	0.000181	0.000180	0.002642	0.002668	0.002667	0.002665
$9B_{1g}$	10.4328	0.000067	-0.000001	-0.000001	0.000054	0.001592	0.001526	0.001525	0.001580
$10A_g$	10.5380	0.000000	-0.000001	-0.000001	-0.000001	0.000211	0.000211	0.000211	0.000211
$11A_g$	10.5445	0.000009	0.000009	0.000010	0.000010	0.000186	0.000186	0.000187	0.000187
$10B_{1g}$	10.5447	0.000009	0.000009	0.000010	0.000009	0.000186	0.000186	0.000186	0.000186
$12B_{2g}$	10.5650	0.000000	0.000000	0.000000	0.000000	0.000000	0.000000	0.000000	0.000000
$12A_g$	10.5817	0.000047	0.000046	0.000045	0.000046	0.000025	0.000020	0.000019	0.000020
$13B_{2g}$	10.6677	0.260047	0.260330	0.260329	0.260619	0.005970	0.007972	0.007974	0.009031
$12B_{3g}$	10.6678	0.259967	0.260249	0.260248	0.260539	0.005968	0.007968	0.007971	0.009027
$13A_g$	10.6743	0.000000	0.000000	0.000002	0.000000	0.000004	0.000005	0.000008	0.000004
$11B_{1g}$	10.6743	0.000000	0.001935	0.001964	0.001577	0.000004	0.001989	0.002018	0.001628
$14B_{2g}$	10.7194	0.000000	0.000000	0.000000	0.000000	0.000000	0.000000	0.000000	0.000000
$15B_{2g}$	10.7567	0.001171	0.001171	0.001171	0.001175	0.000027	0.000024	0.000025	0.000046
$13B_{3g}$	10.7567	0.001185	0.001277	0.001278	0.001274	0.000027	0.000095	0.000097	0.000105

$14B_{3g}$	10.7705	0.000000	0.000000	0.000000	0.000000	0.000000	0.000000	0.000000	0.000000
$15B_{3g}$	10.7982	0.000000	0.000000	0.000000	0.000000	0.000000	0.000000	0.000000	0.000000
$16B_{2g}$	10.8502	0.009982	0.010195	0.010195	0.010163	0.000255	0.000073	0.000074	0.000066
$16B_{3g}$	10.8502	0.009976	0.010203	0.010203	0.010173	0.000255	0.000081	0.000083	0.000075
$17B_{2g}$	10.9490	0.000000	0.000000	0.000000	0.000000	0.000000	0.000000	0.000000	0.000000
$17B_{3g}$	10.9721	0.000000	0.000000	0.000000	0.000000	0.000000	0.000000	0.000000	0.000000
$18B_{2g}$	10.9865	0.032881	0.033081	0.033081	0.033323	0.000763	0.001534	0.001533	0.002050
$18B_{3g}$	10.9866	0.032878	0.032961	0.032961	0.033090	0.000763	0.001302	0.001301	0.001696
$14A_g$	11.1537	0.000000	0.000000	0.000000	0.000000	0.000000	0.000000	0.000001	0.000000
$12B_{1g}$	11.1537	0.000000	0.000136	0.000139	0.000172	0.000000	0.000142	0.000145	0.000179
$19B_{3g}$	11.2302	0.001040	0.001433	0.001434	0.001449	0.000158	0.000725	0.000726	0.000744
$19B_{2g}$	11.2303	0.001044	0.001528	0.001529	0.001536	0.000158	0.000833	0.000834	0.000843
$13B_{1g}$	11.6691	0.000017	-0.000005	-0.000005	0.000020	0.000222	0.000197	0.000197	0.000225
$15A_g$	11.7047	0.000016	0.000016	0.000017	0.000016	0.000246	0.000246	0.000247	0.000246
$14B_{1g}$	11.7047	0.000016	0.000112	0.000113	0.000113	0.000246	0.000339	0.000340	0.000340
$20B_{2g}$	11.7221	0.000000	0.000000	0.000000	0.000000	0.000000	0.000000	0.000000	0.000000
$20B_{3g}$	11.7253	0.000000	0.000000	0.000000	0.000000	0.000000	0.000000	0.000000	0.000000
$16A_g$	11.7369	0.000026	0.000025	0.000025	0.000025	0.000148	0.000148	0.000148	0.000148
$17A_g$	11.9085	0.000000	0.000001	0.000001	0.000001	0.000008	0.000008	0.000008	0.000008
$15B_{1g}$	11.9085	0.000000	0.000005	0.000005	0.000006	0.000008	0.000011	0.000012	0.000012
$18A_g$	12.0279	0.000029	0.000025	0.000022	0.000029	0.000403	0.000400	0.000396	0.000404
$16B_{1g}$	12.0280	0.000029	0.000025	0.000022	0.000029	0.000403	0.000399	0.000396	0.000403
$17B_{1g}$	12.0444	0.000026	0.000101	0.000101	0.000121	0.000246	0.000332	0.000332	0.000353
$19A_g$	12.0625	0.000071	0.000069	0.000068	0.000071	0.000212	0.000212	0.000212	0.000212
$20A_g$	12.2422	0.000021	0.000018	0.000015	0.000023	0.000975	0.000975	0.000974	0.000976
$18B_{1g}$	12.2422	0.000021	0.000728	0.000738	0.000792	0.000974	0.001903	0.001914	0.001974
$21A_g$	12.2499	0.000079	0.000078	0.000076	0.000079	0.001827	0.001828	0.001828	0.001827
$19B_{1g}$	12.3694	0.000004	0.000008	0.000008	0.000000	0.000473	0.000470	0.000469	0.000480
$20B_{1g}$	12.5895	0.000014	0.000013	0.000014	0.000014	0.000459	0.000458	0.000458	0.000458

3.3. *para*-Nitroaniline

TABLE S5: fc-CVS-EOM-EE-CCSD/6-311(2+,+)G**(uC) valence excitation energies $\mathcal{E}_f - \mathcal{E}_0$ (eV) and RIXS cross sections σ (a.u.) for the incident photon resonant with the lowest $XA_1 \rightarrow B_2$ core excitation at 285.88 eV and scattering angle $\theta = 0^\circ$ with the CVS-0, CVS-CCS, CVS-uS, and CVS-CC2 approaches.

		CVS-0	CVS-CCS	CVS-uS	CVS-CC2
Final state	$\mathcal{E}_f - \mathcal{E}_0$	σ	σ	σ	σ
XA_1	0.0000	0.028742	0.027810	0.028133	0.028249
$1A_2$	4.1456	0.000002	0.000002	0.000002	0.000017
$1B_1$	4.6432	0.000000	0.000311	0.000311	0.000112
$2A_1$	4.6632	-0.000001	0.000000	0.000054	0.000004
$1B_2$	4.6799	0.000082	0.000154	0.000154	0.000237
$2B_2$	5.1217	0.000007	0.000020	0.000020	0.000030
$2A_2$	5.9099	0.000038	0.000063	0.000062	0.000061
$2B_1$	5.9626	0.000000	0.001045	0.001048	0.000361
$3B_2$	6.0734	0.000013	0.000010	0.000009	0.000007
$3A_1$	6.4221	0.000049	0.000050	0.000062	0.000050
$3B_1$	6.4575	0.000000	0.001394	0.001393	0.000021
$4B_2$	6.7907	0.000021	0.000107	0.000108	0.000080
$3A_2$	6.8519	0.000004	0.000061	0.000061	0.000087
$4A_2$	6.9513	0.000046	0.000031	0.000028	0.000033
$4A_1$	7.1581	0.000013	0.000019	0.000034	0.000015
$5B_2$	7.2104	0.000001	0.000180	0.000181	0.000114
$5A_1$	7.3305	0.000024	0.000024	0.000024	0.000025
$6B_2$	7.4867	0.000000	0.000000	0.000000	0.000001

3.4. Basis-set dependence of the RIXS spectrum of *para*-nitroaniline

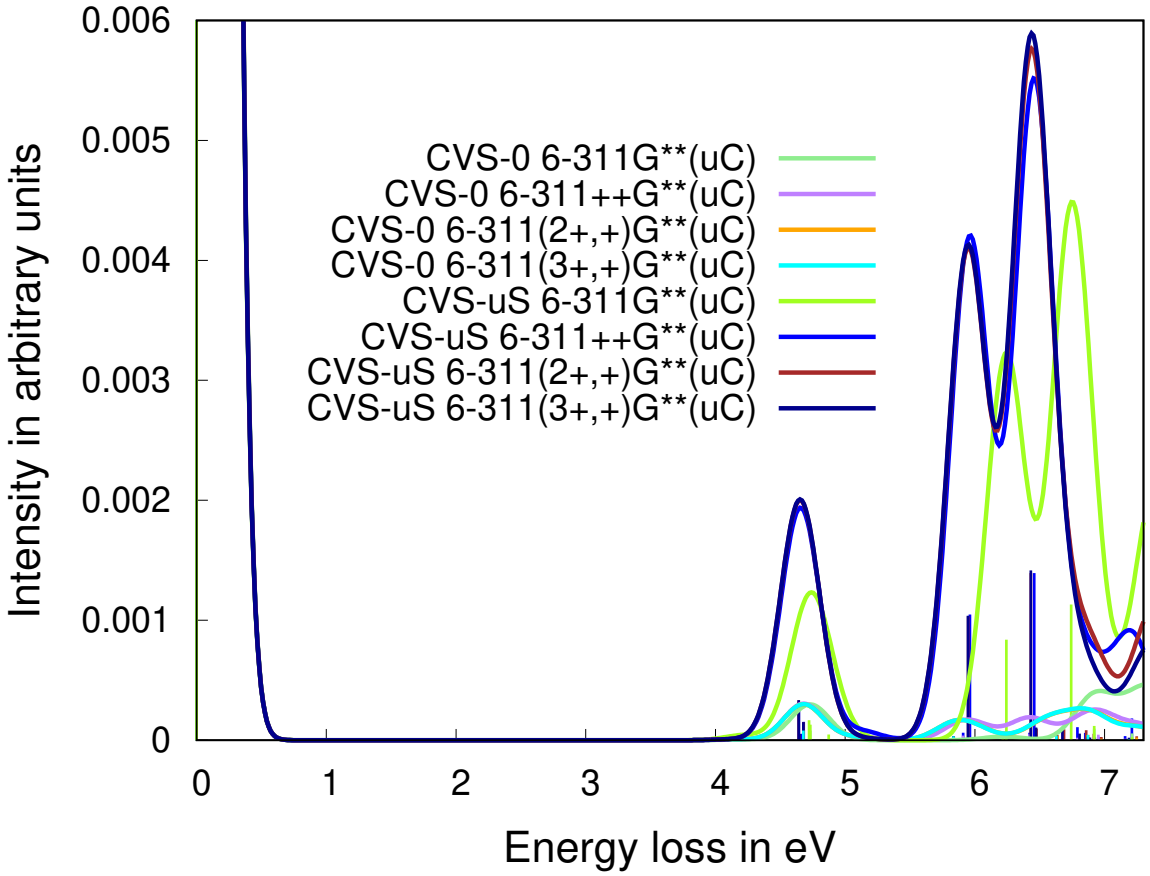

FIG. S3: Basis-set dependence of the RIXS emission spectra for *para*-nitroaniline computed with the CVS-0 and CVS-uS approaches. The spectra are convoluted using normalized Gaussians (FWHM = 0.25 eV).

We investigate the effect of the basis set, in particular, diffuse functions, which are known to be important for modeling two-photon absorption[7]. Fig. S3 shows the RIXS spectra for *para*-nitroaniline computed with CVS-0 and CVS-uS and using the uC-6-311G**, uC-6-311(+,+)G**, uC-6-311(2+,+)G**, and uC-6-311(+,+)G** basis sets. As one can see, the addition of the second and the third set of diffuse functions has negligible effect, indicating that the RIXS spectra are converged with uC-6-311(+,+)G**. In contrast, calculation with the uC-6-311G** basis yields very different spectra. These results indicate that the effect of the valence contributions appear to be relatively insensitive to the basis, provided that at least one set of diffuse functions is included.

4. XAS ENERGIES AND OSCILLATOR STRENGTHS

4.1. *para*-Nitroaniline

TABLE S6: fc-CVS-EOM-EE-CCSD/6-311(2+,+)G**(uC) core excitation energies (eV) and oscillator strengths (f). Only the bright transitions are shown. "c" denotes a core state at the C K-edge.

Final state	Exci. E	f
c1A_1	287.9624	0.0044
c2A_1	288.7944	0.0032
c3A_1	289.0088	0.0002
c4A_1	289.3052	0.0001
c5A_1	289.6468	0.0020
c6A_1	289.6660	0.0007
c7A_1	289.7694	0.0014
c8A_1	289.8582	0.0000
c1B_1	287.9615	0.0146
c2B_1	288.7943	0.0092
c3B_1	289.0089	0.0048
c4B_1	289.3054	0.0025
c5B_1	289.6558	0.0060
c6B_1	289.7696	0.0009
c7B_1	289.8584	0.0004
c8B_1	290.0992	0.0014
c1B_2	285.8807	0.1074
c2B_2	286.2325	0.0839
c3B_2	286.8588	0.0227
c4B_2	287.1942	0.0065
c5B_2	287.3926	0.0595
c6B_2	288.0061	0.0008
c7B_2	289.1258	0.0274
c8B_2	289.9017	0.0065

5. CARTESIAN COORDINATES

5.1. Water

1	O	0.0000000000	0.0000000000	0.1164677113
2	H	-0.7559090748	-0.0000000000	-0.4658708454
3	H	0.7559090748	-0.0000000000	-0.4658708454

Nuclear Repulsion Energy = 9.22316331 hartrees

5.2. Benzene

1	H	2.4750347531	0.0000000000	-0.0000000000
2	C	1.3935929418	0.0000000000	-0.0000000000
3	C	0.6967964709	1.2068868901	0.0000000000
4	H	1.2375173766	2.1434429715	0.0000000000
5	C	-0.6967964709	1.2068868901	0.0000000000
6	H	-1.2375173766	2.1434429715	0.0000000000
7	C	-1.3935929418	0.0000000000	0.0000000000
8	H	-2.4750347531	0.0000000000	0.0000000000
9	C	-0.6967964709	-1.2068868901	-0.0000000000
10	H	-1.2375173766	-2.1434429715	-0.0000000000
11	C	0.6967964709	-1.2068868901	-0.0000000000
12	H	1.2375173766	-2.1434429715	-0.0000000000

Nuclear Repulsion Energy = 203.71874490 hartrees

5.3. *para*-Nitroaniline

1	C	0.0000000000	0.0000000000	0.7153356937
2	C	1.2195927633	0.0000000000	0.0255507248
3	C	1.2182354930	0.0000000000	-1.3699791187
4	C	0.0000000000	0.0000000000	-2.0937199737
5	C	-1.2182354930	0.0000000000	-1.3699791187
6	C	-1.2195927633	0.0000000000	0.0255507248
7	H	2.1553754221	0.0000000000	0.5869226624
8	H	2.1689860113	0.0000000000	-1.9130375835
9	H	-2.1689860113	0.0000000000	-1.9130375835
10	H	-2.1553754221	0.0000000000	0.5869226624
11	N	0.0000000000	0.0000000000	-3.4666053646
12	N	0.0000000000	0.0000000000	2.1848883212
13	O	-1.0841264669	0.0000000000	2.7496493313
14	O	1.0841264669	0.0000000000	2.7496493313
15	H	-0.8656098383	0.0000000000	-3.9833468735
16	H	0.8656098383	0.0000000000	-3.9833468735

Nuclear Repulsion Energy = 493.65919820 hartrees

6. BASIS SETS

6.1. 6-311(+,+)G** basis set with uncontracted core

```
H     0
S   3   1.00
     33.86500                0.0254938
      5.094790               0.190373
      1.158790               0.852161
S   1   1.00
      0.325840               1.000000
S   1   1.00
      0.102741               1.000000
S   1   1.00
      0.0360000              1.0000000
P   1   1.00
      0.750                  1.000000
****
C     0
S   1   1.00
   4563.240                  0.00196665
S   1   1.00
    682.0240                 0.0152306
S   1   1.00
    154.9730                 0.0761269
S   1   1.00
     44.45530                0.2608010
S   1   1.00
     13.02900                0.6164620
S   1   1.00
      1.827730               0.2210060
SP   3   1.00
     20.96420                0.114660               0.0402487
      4.803310               0.919999               0.237594
      1.459330              -0.00303068             0.815854
SP   1   1.00
      0.4834560              1.000000               1.000000
SP   1   1.00
      0.1455850              1.000000               1.000000
SP   1   1.00
      0.0438000              1.0000000              1.0000000
D   1   1.00
      0.626                  1.000000
****
N     0
S   1   1.00
   6293.480                  0.00196979
```

```
S   1   1.00
    949.0440                0.0149613
S   1   1.00
    218.7760                0.0735006
S   1   1.00
     63.69160               0.2489370
S   1   1.00
     18.82820               0.6024600
S   1   1.00
      2.720230              0.2562020
SP   3   1.00
     30.63310               0.111906              0.0383119
      7.026140              0.921666              0.237403
      2.112050             -0.00256919            0.817592
SP   1   1.00
      0.684009              1.000000              1.000000
SP   1   1.00
      0.200878              1.000000              1.000000
SP   1   1.00
      0.0639000             1.0000000             1.0000000
D   1   1.00
      0.913                 1.000000
****
O     0
S   1   1.00
   8588.500                 0.00189515
S   1   1.00
   1297.230                 0.0143859
S   1   1.00
    299.2960                0.0707320
S   1   1.00
     87.37710               0.2400010
S   1   1.00
     25.67890               0.5947970
S   1   1.00
      3.740040              0.2808020
SP   3   1.00
     42.11750               0.113889              0.0365114
      9.628370              0.920811              0.237153
      2.853320             -0.00327447            0.819702
SP   1   1.00
      0.905661              1.000000              1.000000
SP   1   1.00
      0.255611              1.000000              1.000000
SP   1   1.00
      0.0845000             1.0000000             1.0000000
D   1   1.00
      1.292                 1.000000
```

6.2. 6-311(2+,+)G** basis set with uncontracted core

```
H     0
S   3   1.00
     33.86500                0.0254938
      5.094790               0.190373
      1.158790               0.852161
S   1   1.00
      0.325840               1.000000
S   1   1.00
      0.102741               1.000000
S   1   1.00
      0.0360000              1.0000000
P   1   1.00
      0.750                  1.000000
****
C     0
S   1   1.00
   4563.240                  0.00196665
S   1   1.00
    682.0240                 0.0152306
S   1   1.00
    154.9730                 0.0761269
S   1   1.00
     44.45530                0.2608010
S   1   1.00
     13.02900                0.6164620
S   1   1.00
      1.827730               0.2210060
SP   3   1.00
     20.96420                0.114660               0.0402487
      4.803310               0.919999               0.237594
      1.459330              -0.00303068             0.815854
SP   1   1.00
      0.4834560              1.000000               1.000000
SP   1   1.00
      0.1455850              1.000000               1.000000
SP   1   1.00
      0.0438000              1.0000000              1.0000000
SP   1   1.000
      0.0131927711           1.0000000              1.0000000
D   1   1.00
      0.626                  1.000000
```

6.3. Basis set used for water

```
H     0
```

```
S   3   1.00
     33.8650000              0.0254938
      5.0947900              0.1903730
      1.1587900              0.8521610
S   1   1.00
      0.3258400              1.0000000
S   1   1.00
      0.1027410              1.0000000
S   1   1.00
      0.0360000              1.0000000
P   1   1.00
      0.7500000              1.0000000
****
O     0
S   6   1.00
   8588.5000000              0.00189515
   1297.2300000              0.0143859
    299.2960000              0.0707320
     87.3771000              0.2400010
     25.6789000              0.5947970
      3.7400400              0.2808020
SP   3   1.00
     42.1175000              0.1138890              0.0365114
      9.6283700              0.9208110              0.2371530
      2.8533200             -0.00327447             0.8197020
SP   1   1.00
      0.9056610              1.0000000              1.0000000
SP   1   1.00
      0.2556110              1.0000000              1.0000000
SP   1   1.00
      0.0845000              1.0000000              1.0000000
D   1   1.00
      1.2920000              1.0000000
S   1   1.00
 0.0058583805        1.0000000000
S   1   1.00
 0.0033459739        1.0000000000
S   1   1.00
 0.0020484225        1.0000000000
P   1   1.00
        0.0099882106        1.0000000000
P   1   1.00
        0.0056893607        1.0000000000
P   1   1.00
 0.0034756797        1.0000000000
```

7. BIBLIOGRAPHY

[1] S. Coriani and H. Koch, J. Chem. Phys. **143**, 181103 (2015).

[2] S. Coriani and H. Koch, J. Chem. Phys. **145**, 149901 (2016).

[3] M. L. Vidal, X. Feng, E. Epifanovski, A. I. Krylov, and S. Coriani, J. Chem. Theory Comput. **15**, 3117 (2019).

[4] K. D. Nanda, M. L. Vidal, R. Faber, S. Coriani, and A. I. Krylov, Phys. Chem. Chem. Phys. **22**, 2629 (2020).

[5] A. Sadybekov and A. I. Krylov, J. Chem. Phys. **147**, 014107 (2017).

[6] K. D. Nanda and A. I. Krylov, J. Chem. Phys. **152**, 244118 (2020).

[7] M. Paterson, O. Christiansen, F. Pawlowski, P. Jørgensen, C. Hättig, T. Helgaker, and P. Salek, J. Chem. Phys. **124**, 054332 (2006).